RSC Mechanochemistry

Accepted Manuscript

This article can be cited before page numbers have been issued, to do this please use: A. S A and B. Sarkarainadar, *RSC Mechanochem.*, 2026, DOI: 10.1039/D6MR00044D.

Energy-efficient mechanochemical synthesis of $MgWO_4$ phase materials: (micro)-structural, thermal, and optical properties

S. A. Ashika[$], S. Balamurugan[1,*,¥]

[1]Advanced Nanomaterials Research Laboratory, Department of Nanotechnology, Noorul Islam Centre for Higher Education, Thuckalay, Kumaracoil - 629 180, India

[*]Correspondence e-mail address: scandium.chemistry@gmail.com

[$]https://orcid.org/0000-0002-0773-0650

[¥]https://orcid.org/0000-0002-7366-3417

Abstract

We prepared $MgWO_4$ phase materials using a single-step energy-efficient mechanochemical approach, which differs from existing studies on the phase formation, thermal, optical, and morphological features. The as-milled powder reveals a monoclinic structure with the lattice parameters, a = 0.4683(5) nm, b = 0.5686(6), c = 0.4956(6) nm, and β = 90.73°. The TGA curve shows a weight loss of 4.7% for the as-milled powder. The IR bands at 513 and 570 cm^{-1} indicate the Mg-O vibration mode, whereas the IR bands seen at 794 and 825 cm^{-1} are assigned to W-O vibration mode for the $MgWO_4$ phase materials. The NIR reflectance of the $MgWO_4$ phase analysis achieved in the present work is novel in comparison to the existing studies, which reveal a maximum reflectance of ~35% in the solar NIR reflectance region. The as-milled powder $MgWO_4$ has the E_g^{direct} of 3.97 eV. Agglomerated particles of $MgWO_4$ phases are observed in the SEM images.

Keywords: $MgWO_4$ phase; Ball-milling method; Monoclinic structure; Optical properties; NIR pigmentation

View Article Online
DOI: 10.1039/D6MR00044D

1. Introduction

The metal tungstates of the AWO_4 series with A^{2+} ions of IIA group elements (Mg, Ca, Sr, Ba) and *d*-block elements (Mn, Fe, Co, Ni, Zn, Cd) attract the researchers owing to their wide range of applications in various sectors / areas [1 - 10]. The AWO_4 series has the tendency to form two crystal structures, such as wolframite and scheelite, that are decided by the ionic radii of the A^{2+} ions. The A^{2+} ions with smaller ionic radii which are less than 0.077 nm form the monoclinic wolframite structure, whereas the A^{2+} ions with larger ionic radii (greater than 0.099 nm) form the tetragonal scheelite structure [1, 2]. For example, A^{2+} ions with Mg, Zn, Co, Cd, Fe, Mn, Ni stabilize the monoclinic wolframite structure. On the other hand, A^{2+} ions with Ca, Sr, Ba, Pb, Eu form the tetragonal scheelite structure. Though the most common AWO_4 type phases of $CaWO_4$, $SrWO_4$, and $BaWO_4$ are well known for its suitability in numerous fields, the $MgWO_4$ phase materials have not been investigated to the extent of the former phases. Thus, our attention is focused on the later one ($MgWO_4$) to explore the new findings. In general, $MgWO_4$ has two phases; α-$MgWO_4$ and β-$MgWO_4$. The α-$MgWO_4$ phase stabilizes in triclinic structure under high temperature, while the β-$MgWO_4$ phase crystallizes in monoclinic structure under 1165°C [3]. Further, Gancheva *et al*. [11] reported that $MgWO_4$ has the tendency to form a tetragonal structure in addition to a triclinic and monoclinic structure when the sample is prepared under lower temperature which range from 400 to 850°C. Several methods have been reported for the synthesis of $MgWO_4$ materials and some of them are solid state reaction method, mechanochemical, single crystal growth, flux method, co-precipitation, hydrothermal, complex polymerization, chemical vapour deposition, flux method, electrospinning, and gamma-ray irradiation [2, 11 - 23]. Some of the notable characteristics of $MgWO_4$ phases are listed in Figure 1. The wide range of applications of $MgWO_4$ are catalysts, scintillators, photoluminescent materials, laser host materials, microwave applications, pigments, and solid-state lasers [2, 12, 19].

View Article Online
DOI: 10.1039/D6MR00044D

Some of the research findings of $MgWO_4$ materials reported by different researchers are compared here. Sota *et al*. [24] prepared $MgWO_4$ materials after heat treatment of the reagents, MgO and WO_3 at 1000°C for 12 h via solid state route. By using a hydrothermal method, the $MgWO_4$ materials were prepared by Meng *et al*. [15] and Hurley *et al*. [25] to study its photocatalytic behavior and photoluminescence and radioluminescence nature, respectively. Further, the existing reports relevant to the synthesis of $MgWO_4$ phase materials based on a ball-milling process are briefed here [1, 11, 20, 22]. Kim *et al*. [20] prepared $MgWO_4$ materials by solid state reaction using the homogenized mixture (MgO and WO_3) by ball milling for 24 hours in ethanol solvent followed by heating at 900°C / 2 h. Gancheva *et al*. [11] have aimed to synthesize the $MgWO_4$ materials through a mechanically activated (500 rpm/5-10 h) mixture of $MgCO_3 \cdot 3H_2O$ and WO_3 and the mixture of MgO and WO_3 in a planetary ball milling machine with the model of Fritsch-Premium line/Pulversette No. 7. The ball milling conditions employed for their work were: ball to powder mass ratio of 10:1. A ball milling duration of 15 minutes was succeeded by a 5-minute pause to prevent an excessive increase in temperature within the grinding chamber. Types of precursors and annealing temperature (600 and 850°C) have influenced the phase formation and purity of the final products [11]. For a microwave dielectric ceramic study, Pullar *et al*. [1] obtained sintered $MgWO_4$ samples at 900 – 1200°C/2h using a ball milled powder made from MgO and WO_3 as a reaction mixture. According to them, the reaction mixture was initially ball milled for 1 day in zirconia milling media in the presence of water and then dried. The dried powder was then calcined at 900°C/12 h and then milled at 300 rpm/3 h using water on a Fritsch Pulverisette ball milling machine. The sintered monoclinic $MgWO_4$ sample was nearly single phase with a second phase at $2\theta = 37.5°$. In accordance with the report of Guo *et al*., the ball-milled powder (made from MgO and WO_3 as a reaction mixture) was obtained using ethanol

View Article Online
DOI: 10.1039/D6MR00044D

as a solvent in a polyethylene jar using zirconia balls at 4 h and subsequent heat treatment at 1000°C / 3 h yield monoclinic $MgWO_4$ phase [22].

In this paper, we have synthesized monoclinic $MgWO_4$ phase materials by the ball-milling method (VBCC, Chennai), despite a few of the reports [1, 11, 22] dealing with ball milling followed by high-temperature treatment. The ball milling conditions employed by us in the present work is quite different as compared to the existing reports. The phase formation, thermal features, optical properties, and morphology were systematically studied, which distinguishes them from previous mechanochemical studies. To our knowledge, hardly any report on the synthesis of $MgWO_4$ phase materials in a single step without the requirement of further heat treatment in the experimental conditions described below (see, section 2). Furthermore, the NIR reflectance of the $MgWO_4$ phase materials study conducted in the present work is novel as compared to the existing studies.

2. Experimental procedure

The starting materials used for the ball-milling experiment were MgO and WO_3. For this experiment, 0.45 (g) of MgO and 2.5885 (g) of WO_3 were ground for 20 mins using agate mortar and pestle. Then the reaction mixture was transferred into the tungsten carbide (WC) jar. In this, 30 WC balls (10 mm diameter), 15 WC balls (8 mm diameter), and 3 WC balls (20 mm diameter) were used for ball milling the reaction mixture at 300 rpm for 10h. After that, the as-milled powder was collected and confirmed the phase purity by X-ray diffraction (XRD) using a Bruker XRD diffractometer with Cu K_α radiation ($\lambda = 0.154046$ nm), scanned over a 2θ angle of 10° – 80° with step size of 0.02° and a counting duration of 0.5 s per step. After confirming the phase purity, different characterization techniques such as thermal gravimetric (TG) and differential thermal analyses (DTA), fourier-transform infrared (FTIR), ultraviolet visible (UV–Vis), near-infrared (NIR) analysis, scanning electron microscope (SEM), and energy dispersive X-ray analyzer

View Article Online
DOI: 10.1039/D6MR00044D

(EDX) were performed in the present work. Thermal behavior was studied using TGA/DTA (TG/DTA6300, EXSTAR series, Seiko Instruments Inc., Japan) under continuous air flow at a heating rate of 20 °C min^{-1}. Diffuse reflectance spectra were recorded between 200 and 2500 nm using a JASCO spectrophotometer with a D2/WI light source. FTIR spectra were obtained in KBr transmittance mode using a Thermo Fisher Scientific Nicolet iS50 spectrometer. The micro-structural images of $MgWO_4$ materials were done using FESEM with a resolution of 1.0 nm at 15 kV, 1.6 nm at 1kV acceleration and a magnification level up to 1,000,000× by the Smart EDX EDS analysis system (Carl Zeiss- Sigma 300, German).

3. Results and discussion

3.1. XRD

Figure 2 represents the XRD patterns of the reaction mixture (left) and the as-milled product (right) of $MgWO_4$ nanomaterials. Interestingly, the as-milled product reveals monoclinic symmetry (P2/c) with the lattice parameters, a = 0.4683(5) nm, b = 0.5686(6), c = 0.4956(6) nm, and β = 90.73°. These values are comparable with other existing reports [12, 22, 24]. According to the report of Guo *et al*. [22], the monoclinic $MgWO_4$ phase with lattice parameters of a = 0.46864 nm, b = 0.56755 nm, and c = 0.49284 nm has been noted for the ball-milled powder consequently heat treatment at 1000°C / 3 h. The $MgWO_4$ powder obtained by a solid-state reaction carried out at 900°C / 4h yielded the lattice parameters of a = 0.4642 nm, b = 0.5594 nm, c = 0.488 nm, and β = 90.56° [12]. Sota *et al*. [24] reported the significance of heating temperature between 850 and 1000°C through solid-state reaction between MgO and WO_3. At higher temperature (1000°C), they could obtain the phase pure $MgWO_4$ materials, while at low temperature (850°C) a couple of weak impurities of WO_3 were observed along with $MgWO_4$ phase [24]. While comparing with the cited ref. [12] of Bhuyan *et al*., an increase in lattice parameters was noted as a = 0.46906 nm, b = 0.56782 nm, and c = 0.49315 nm [24]. This may be

due to the difference in synthesis methods and conditions. $MgWO_4$ single crystals grown using $K_2W_2O_7$ as a flux by the effective TSSG method [18] revealed the lattice parameters of a = 0.4686(7) nm, b = 0.5674(1) nm, c = 0.4927(8) nm, and β = 90.710(7)°.

The average crystalline size, D, was calculated as 12.6 nm and 17.07 nm from Debye-Scherrer and Williamson-Hall (W-H) methods [26 - 28] for the present as-milled powder of $MgWO_4$ phase materials (see, Figure 3), whereas the electrospinning of $(CH_3COO)_2Mg{\cdot}4H_2O$, $(NH_4)_6W_7O_{24}{\cdot}4H_2O$), and PVA as precursors revealed D of 69.8 nm upon calcining the as-obtained fibers at 700°C/3 h [2]. This monoclinic phase had the structural values of a = 0.465 nm, b = 0.564 nm, and c = 0.49 nm [2]. On the other hand, D = 24.63 nm was revealed for the tetragonal $MgWO_4$ phase, which was obtained by a modified-combustion method using $Mg(NO_3)_2.6H_2O$, $(NH_4)_6W_{12}O_{39}.2H_2O$, and citric acid upon calcining the as-prepared product at 600°C/1 h [29]. The formation of the tetragonal $MgWO_4$ phase is mainly based on the difference in the synthesis methods/conditions, precursors, and heat/radiation treatments. This tetragonal phase forms at relatively lower synthesis temperatures [11, 13, 15, 29].

The sample having the oxides of MgO and WO_3 after ball milling for 10 h and subsequent heat treatment at 600°C revealed the mixture of tetragonal and monoclinic $MgWO_4$ phases, MgO, and WO_3 as evidenced from the XRD patterns [11]. At 850°C, the monoclinic $MgWO_4$ phase along with an impurity of the WO_3 phase has been formed [11]. Further, the XRD patterns of the sample containing $MgCO_3.3H_2O$ and WO_3 after 10 h milling time and thermal treatment at 600° C yielded a pure tetragonal $MgWO_4$ phase, and at 850°C pure monoclinic $MgWO_4$ phase have been formed [11]. The radiation flux synthesis of tetragonal $MgWO_4$ materials [13], which involved the direct application of a high energy electron flux of 1.4 MeV with a flux power density of 15 and 18 kW/cm^2 directed at the powder mixture made from MgO and WO_3. Template-free

View Article Online
DOI: 10.1039/D6MR00044D

hydrothermal synthesis of $MgWO_4$ nanoplates revealed the tetragonal phase of $MgWO_4$ with a = 0.563 nm and c = 1.081 nm [15].

3.2. TG/DTA

Figure 4 shows the TGA and DTA plots of the reaction mixture (left) and as-milled powder (right) of $MgWO_4$ materials, which resulted in weight losses of 2.6% and 4.7%, respectively. The slightly increased weight loss seen in the as-milled powder may be due to the formation of the desired $MgWO_4$ phase, as the planetary ball milling machine works on the combination of friction, shear, and impacts are subsequently produced. The slight increase in weight loss seen in the as-milled $MgWO_4$ powder may be due to the surface-related effects induced by mechanical milling. Further, this may be owing to the presence of surface adsorption related to physisorbed water and surface OH^- species in the as-milled powder [30]. The review article by Amrute *et al.* [30] highlighted that low-temperature (<200°C) weight loss is a signature of physisorbed water and surface OH^- species in the as-milled inorganic powder [30]. The saturation in weight loss in the as-milled powder started at 660°C. The DTA curves of the reaction mixture and the as-milled $MgWO_4$ materials witnessed no endo- and exothermic events. The absence of endo/exothermic peaks in the DTA curve of the as-milled powder implies that the mechanochemical treatment of the reaction mixture at 300 rpm for 10 h had completed the formation of the $MgWO_4$ phase during milling. Subsequently, no additional thermal events were detected during successive heating in the thermal analysis. Mechanochemical milling develops interfacial contact between the precursors of MgO and WO_3, thus considerably enhancing the reactivity of the reaction mixture. Such mechanochemical activation can promote direct formation of the $MgWO_4$ phase. This finding supports the efficiency of mechanochemical milling in achieving phase formation without the need for additional thermal activation. The absence of endo/exothermic peaks in the DTA curve may also be ascribed to the nanocrystalline nature of the as-milled powder. Among the cited

View Article Online
DOI: 10.1039/D6MR00044D

references, there are hardly any reports found for the TGA analysis of $MgWO_4$ phase materials. However, in order to find out the phase formation temperature, Gancheva *et al*. [11] conducted DTA analysis between room temperature and 1000°C for the mixture of MgO and WO_3 following a milling duration of 10 hours. The DTA curve showed multiple exothermal peaks at temperatures of 530, 630, 920, and 960°C. Among these, the peaks observed at 530 and 630°C are associated with the formation of the $MgWO_4$ phase.

3.3. UV-Vis-NIR spectral features

The UV-Vis absorbance spectrum in Figure 5 (left) exhibits a well-defined absorption maximum (λ^{max}) peak at 257 nm and the estimation of optical energy gap (E_g) of the $MgWO_4$ phase materials from the Kubelka-Munk (K-M) model is represented in Figure 5 (right). The $MgWO_4$ phase materials obtained by Wang *et al.* [19] and Meng *et al.* [15] revealed a λ^{max} peak at ~250 nm [19] and at ~260 nm [15], respectively. This main absorption edge/peak (λ^{max}) is related to the electronic transitions from the valence band (O 2p states) to the conduction band (W 5d orbital), which are mainly related to the intra-group transitions within the $[WO_4]^{2-}$ complex in $MgWO_4$ structure [12, 16]. The E_g of the $MgWO_4$ phase powder is estimated from the Tauc equation and the K-M model, which is derived from the absorbance and/or reflectance data obtained from DRS measurements for direct transition in band gap [12, 15, 16, 19, 31]. The E_g^{direct} of 3.97 eV determined by KM model for the present $MgWO_4$ phase materials is compared with the existing reports. The $MgWO_4$ phase has been found to show E_g values ranging from ~3.8 to 4.33 eV with the direct assignments varying among different reports, synthesis methods and conditions, phase formation, and analytical methods [12, 15, 16, 19, 31]. The absorption spectrum obtained from UV-visible analysis exhibited a E_g^{direct} of 4.17 eV [12]. The UV-vis DRS spectra of $MgWO_4$ samples synthesized through a single-step hydrothermal method, exhibiting various morphologies such as nanoplate shapes and nanoparticle structures, exhibited comparable optical

View Article Online
DOI: 10.1039/D6MR00044D

absorption ranges or edges [15]. The estimated E_g of the tetragonal $MgWO_4$ nanoparticles and nanoplates, as determined by the Tauc method, was found to be 4.15 and 4.10 eV, respectively [15]. The UV–Vis spectra and the E_g values of the $MgWO_4$ phases, which were obtained by a γ-ray irradiation method, showed variations in absorbance features and E_g values upon calcining of the as-prepared powder at various temperatures (400 – 900°C) [19]. The reported E_g values were determined to be 4.07, 3.65, 2.82, 3.73, 4.03, and 3.54 eV for the calcination of the as-prepared powder at 400, 500, 600, 700, 800, and 900°C, respectively [19]. Dey *et al.* [31] have analyzed the optical properties and electronic structures of $MgWO_4$ materials obtained via a solid-state reaction method. In this compound, the E_g value is 4.06 eV [31]. Gouveia *et al.* [16] synthesized $MgWO_4$ powder by the complex polymerization method upon heat-treating the intermediate product at 900°C/2 h. For this synthesized $MgWO_4$ powder, they obtained E_g^{direct} of 4.33 eV using the KM model, while the band structure calculation showed an E_g^{direct} value of 4.49 eV. This difference is ascribed to the presence of localized electronic levels within the forbidden E_g [16]. The intense absorption in the UV region and wideband gap indicate that the material could be a promising candidate for applications in photoluminescence, laser host materials, pigments, and scintillators [31, 32, 33].

The scheelites and their derivative materials [34 - 43] have been found to exhibit significant reflectance in the near infrared (NIR) range between 750 and 2500 nm, which varies depending upon the phase compositions and the methods and conditions of synthesis (see, Table 2). These NIR spectral features make them suitable for applications in solar reflective pigments and the NIR color pigmentation industry. However, there is a lack of reports regarding the NIR spectrum of $MgWO_4$ phase materials within these NIR regions. In the present work, the as-milled powder of monoclinic $MgWO_4$ phase materials exhibits a maximum NIR reflectance of ~35 % in the region between 750 and 1350 nm (Figure 6). The observed relatively low reflectance of the

View Article Online
DOI: 10.1039/D6MR00044D

as-milled powder could be attributed to the stress generated during the ball milling process of the reaction mixture. A decrease in NIR reflectance has been reported for various oxide-based materials produced through the ball-milling process [44 - 46]. It is quite interesting to compare with our previous work on the $CaMoO_4$ phase [42], which showed relatively lower NIR reflectance of 37% (similar to the current $MgWO_4$ phase), whereas the co-precipitated ($CaMoO_4$) product showed a higher NIR reflectance of □85%. We believe that the reduced NIR reflectance of the ball-milled product is owing to the stress-induced by ball-milling of the reaction mixture [42]. Furthermore, the reduced particle size by ball-milling would increase the surface area, which enhances the scattering mechanism, thereby reducing the reflectance of the materials.

3.4. FTIR spectrum

The FTIR spectrum of $MgWO_4$ phase materials (Figure 7) reveals IR bands at 3263, 1631, 825, 794, 570, and 513 cm^{-1} in the range between 4000 and 400 cm^{-1}. The IR bands seen at 513 and 570 cm^{-1} are associated with the Mg-O vibration mode. The IR bands of 794 and 825 cm^{-1} are related to W-O vibration mode. In addition to these main IR bands, the IR bands attributable to adsorbed water were also seen at 1631 cm^{-1} (bending mode) and 3263 cm^{-1} (stretching mode), validating the presence of adsorbed moisture and OH^- species which is reflected in the TGA curve (Fig. 4(right)) of as-milled $MgWO_4$ powder showing weight loss in the lower temperature region (below 350°C). These observed IR band assignments are corroborated with the reports on the $MgWO_4$ phase materials [11, 12, 19, 29]. The transmittance curves of $MgWO_4$ materials shown in the report of Bhuyan *et al.* [12] illustrate the intense IR bands in the wavenumber ranges between 400 and 900 cm^{-1} and a weak band at 1022 cm^{-1} which is due to the vibrational peak of $CO3^{2-}$ species. The intense IR peaks located at 435, 501, and 549 cm^{-1} correspond to the Mg-O vibration mode and the band at 783 and 879 cm^{-1} are attributed to O-W-O vibration mode and W-O stretching mode, respectively. In another report [29], the tetragonal $MgWO_4$ phase materials

View Article Online
DOI: 10.1039/D6MR00044D

obtained via a modified combustion method show the IR bands at 856, 794, and 743 cm^{-1}, which are attributed to W-O asymmetric stretching mode, whereas the IR bands located at 474, 398, and 384 cm^{-1} are corresponding to O-W-O asymmetric bending mode. The observed IR bands at 647 and 413 cm^{-1} are due to Mg-O stretching vibrations [29].

3.5. Morphology

The morphological features related to $MgWO_4$ phase materials are confirmed from Figure 8. It reveals the nanostructures of particles are agglomerates of smaller crystallites and EDX pattern which confirm the presence of Mg, W, and O in the studied materials. Generally, the ball-milled powder has the tendency of showing agglomerated particles in variety of oxide-based nanomaterials that exist in many reports in literature. Monoclinic $MgWO_4$ particles with different sizes and shapes have been noticed in the TEM images for the $MgWO_4$ materials obtained through mechanically activated (500 rpm/5-10 h) mixture of $MgCO_3 \cdot 3H_2O$ and WO_3 [11]. Their obtained size of the $MgWO_4$ particles (~120 nm) by TEM is in accordance with the XRD average crystalline size of 100 nm [11]. According to the report of Pullar *et al*. [1], the $MgWO_4$ samples obtained at 900 - 1200°C/2h through ball milling followed by sintering revealed well sintered grains with low density at 950°C, while very large grains were grown at high temperature (1200°C) [1]. In another work, ball milling followed by heat treatment at 1000°C / 3 h showed dense microstructures of rod-shaped grains and blocky ones with the grain sizes of 3 – 10 μm [22]. Further, various microstructural features have been reported for the $MgWO_4$ samples obtained through different synthesis methods (Table 1). Densely arranged microcrystals revealing polyhedral shapes with typical dimensions of 2 - 5μm are reported for the $MgWO_4$ phase materials crystallized in tetragonal structure via radiation flux method [13]. Plate-like nanostructures that possess an irregular morphology with a thickness of ~ 45 nm has been reported for the tetragonal $MgWO_4$ phase materials obtained by hydrothermal method [15].

View Article Online
DOI: 10.1039/D6MR00044D

4. Conclusion

We presented a simple, solvent-free, and energy-efficient mechanochemical approach for synthesizing phase-pure monoclinic $MgWO_4$ materials using a mixture of MgO and WO_3, which has a D value as 12.6 nm without post-annealing treatment. This approach is easy, cost-effective, and potentially scalable, producing nanoscale crystallites with structural stability and optical properties comparable to previously reported methods. The as-milled powder revealed the weight loss of 4.7% as evidenced by TGA. The absence of endo/exothermic peaks in the DTA curve indicates that the $MgWO_4$ phase is formed during mechanochemical milling, which is reminiscent of the ball-milled $CaWO_4$ phase materials [43]. The FTIR spectrum of $MgWO_4$ phase materials revealed IR bands at 513 and 570 cm^{-1} correlated to the Mg-O vibration mode and the IR bands at 794 and 825 cm^{-1} are related to W-O vibration mode. UV-Vis absorbance spectrum revealed a distinct λ^{max} peak at 257 nm. The KM model which is accompanying with the Tauc relation yielded the E_g^{direct} of 3.97 eV. FESEM analysis showed the nanostructure of agglomerated particles. The reported NIR reflectance (around 35%) is moderate, which can be significantly improved by tuning by various synthesis methods and processing conditions. For cool roof or solar-reflective pigment applications, commercial cool pigments typically exhibit significantly higher NIR reflectance. Thus, an extensive work on the $MgWO_4$ materials could bring out the insight of the NIR reflectance.

Acknowledgments

The author, S. A. Ashika is indebted to the award of DST- INSPIRE Fellowship (Offer letter No: DST/INSPIRE Fellowship/[IF230137]), GOVERNMENT OF INDIA, MINISTRY OF SCIENCE and TECHNOLOGY, Department of Science and Technology, Technology Bhawan, New Mehrauli Road, New Delhi – 110016) to conduct the research work under the guidance of Prof. Dr. S. Balamurugan, Department of Nanotechnology, Noorul Islam Centre for Higher Education.

View Article Online
DOI: 10.1039/D6MR00044D

The authors thank the reviewers for providing their valuable comments/suggestions for significant improvements to the manuscript.

Conflict of interest

The authors state that there is no conflict of interest.

Funding

Not applicable

CRediT statement

S.A. Ashika: Data Curation; Formal Analysis; Investigation; Methodology; Resources; Validation; Writing – Original Draft Preparation; Writing – review and editing.

S. Balamurugan: Supervision; Conceptualization; Data Curation; Formal Analysis; Methodology; Resources; Project Administration; Validation; Visualization; Writing – Original Draft Preparation; Writing – review and editing.

Data Availability Statement

All relevant data generated and analyzed during this study are included in this article.

View Article Online
DOI: 10.1039/D6MR00044D

References

1. R. C. Pullar, S. Farrah and N. M. Alford, $MgWO_4$, $ZnWO_4$, $NiWO_4$ and $CoWO_4$ microwave dielectric ceramics, *J. Eur. Ceram. Soc.,* 2007, 27, 1059-1063, DOI: 10.1016/j.jeurceramsoc.2006.05.085

2. S. Wannapop, T. Thongtem and S. Thongtem, Photoemission and energy gap of $MgWO_4$ particles connecting as nanofibers synthesized by electrospinning–calcination combinations, *Appl. Surf. Sci.*, 2012, 258, 4971-4976, DOI: 10.1016/j.apsusc.2012.01.133

3. J. Jayaprakash and V. Krishnakumar, Synthesis and optical characterization of cerium doped $MgWO_4$ phosphor, *Mater. Today: Proc.*, 2020, 26, 3514-3517, DOI: 10.1016/j.matpr.2019.05.385

4. R. Iordanova, M. Gancheva, I. Koseva, G. Avdeev and P. Ivanov, Synthesis, Characterization and Optical Behavior of Nanocrystalline $CoWO_4$, *Molecules*, 2025, *30*, 3843, DOI: 10.3390/molecules30193843

5. D. Diaz-Anichtchenko, J. E. Aviles-Coronado, S. López-Moreno, R. Turnbull, F. J. Manjon, C. Popescu and D. Errandonea, Electronic, vibrational, and structural properties of the natural mineral ferberite ($FeWO_4$): A high-pressure study, *Inorg. Chem.*, 2024, *63*, 6898-6908, DOI: 10.1021/acs.inorgchem.4c00345

6. Y. Yu, D. Cheng, J. Dong, Z. Yao, L. Zhang, Y. Xu, Y. Shen, J. Zhao, H. Liu, F. Shi and Z. M. Qi, Crystal structures, lattice vibrational characteristics, and dielectric responses of $ZnWO_4$ microwave dielectric ceramics sintered at different temperatures, *Mater. Sci. Eng., B*, 2024, *309*, 117647, DOI: 10.1016/j.mseb.2024.117647

7. R. Iordanova, M. Gancheva, I. Koseva, P. Tzvetkov and P. Ivanov, The Influence of High-Energy Milling on the Phase Formation, Structural, and Photoluminescent Properties of $CaWO_4$ Nanoparticles, *Materials*, 2024, 17, 3724, DOI: 10.3390/ma17153724

8. N. Heydarian Dehkordi, M. Raeisi and S. Alamdari, Exploring the Enhanced Optical and Antibacterial Properties of Ag-Doped $CdWO_4$ Nanopowders: Synthesis, Characterization, and Multifaceted Applications, *Nanochem Res.*, 2024, *9*, 248-261, DOI: 10.22036/NCR.2024.04.01

9. A. Alruwaili and M. S. Shalaby, The impact of $NiWO_4$ on the enhancement of structural, optical, and radiation shielding properties of PVC nanocomposite films, *J. Mater. Sci.: Mater. Electron.*, 2024, *35*, 2170, DOI: 10.1007/s10854-024-13932-3

10. D. Diaz-Anichtchenko, J. Ibáñez, P. Botella, R. Oliva, A. Kuzmin, L. Wang, Y. Li, A. Muñoz, F. Alabarse and D. Errandonea, Identification of the high-pressure phases of α-$SnWO_4$ combining x-ray diffraction and crystal structure prediction, *Physica B: Condensed Matter*, 2025, 696, 416666, DOI: 10.1016/j.physb.2024.416666

11. M. Gancheva, A. Naydenov, R. Iordanova, D. Nihtianova and P. Stefanov, Mechanochemically assisted solid state synthesis, characterization, and catalytic properties of MgWO4, *J. Mater. Sci.*, 2015, 50, 3447-3456, DOI: 10.1007/s10853-015-8904-5

12. P. D. Bhuyan, D. Singh, S. Kansara, P. Yadav, S. K. Gupta, Y. Sonvane, S. K. Rout and E. Sinha, Experimental and theoretical analysis of electronic and optical properties of $MgWO_4$, *J. Mater. Sci.*, 2017, 52, 4934-4943, DOI: 10.1007/s10853-016-0730-x

13. G. Alpyssova, V. Lisitsyn, Z. Bakiyeva, I. Chakin, E. Kaneva, D. Afanasyev, A. Tussupbekova, V. Vaganov, A. T. Tulegenova and S. Tuleuov, Characterization of $ZnWO_4$, $MgWO_4$, and $CaWO_4$ Ceramics Synthesized in the Field of a Powerful Radiation Flux, *Ceramics*, 2024, 7, 1085-1099, DOI: 10.3390/ceramics7030071

14. E. Hildebrandt, V. Kahlenberg, H. Krueger, S. Wagner, D.F. Dinu, T.S. Hofer, P. Tropper and K. Liedl, Structural and computational studies on a quenchable high-temperature polymorph of magnesium tungstate ($MgWO_4$-II), *J. Solid State Chem.*, 2023, 327, 124269, DOI: 10.1016/j.jssc.2023.124269

15. J. Meng, T. Chen, X. Wei, J. Li and Z. Zhang, Template-free hydrothermal synthesis of $MgWO_4$ nanoplates and their application as photocatalysts, *RSC Adv.*, 2019, 9, 2567-2571, DOI: 10.1039/C8RA06671J

16. A.F. Gouveia, V. E. M. Vieira, J. C. Sczancoski, P. S. Lemos, S. K. Rout, N. S. Arul, E. Longo and L. S. Cavalcante, Electronic structure, morphological aspects, and photocatalytic discoloration of three organic dyes with $MgWO_4$ powders synthesized by the complex polymerization method, *J. Inorg. Organomet. Polym. Mater.*, 2020, 30, 2952-2970, DOI: 10.1007/s10904-019-01435-2

17. X. Feng, W. Feng, M. Xia, K. Wang, H. Liu, D. Deng, X. Qin, W. Yao and W. Zhu, Co-precipitation synthesis, photoluminescence properties and theoretical calculations of $MgWO_4$: Eu^{3+} phosphors, *RSC Adv.,* 2016, 6, 14826-14831, DOI: 10.1039/C5RA22631G

18. G.Z. Elabedine, R.M. Solé, S. Slimi, M. Aguiló, F. Díaz, W. Chen, V. Petrov and X. Mateos, Growth, anisotropy, and spectroscopy of Tm^{3+} and Yb^{3+} doped $MgWO_4$ crystals, *CrystEngComm*, 2025, 27, 1619-1631, DOI: 10.1039/D4CE01168F

19. S. Wang, H. Gao, C. Chen, Q. Li, C. Li, Y. Wei and L. Fang, Effect of phase transition on optical and photoluminescence properties of nano-$MgWO_4$ phosphor prepared by a gamma-ray irradiation assisted polyacrylamide gel method, *J. Mater. Sci.: Mater. Electron.*, 2019, 30, 15744-15753, DOI: 10.1007/s10854-019-01960-3

20. D. W. Kim, I. S. Cho, S. S. Shin, S. Lee, T. H. Noh, D. H. Kim, H. S. Jung and K. S. Hong, Electronic band structures and photovoltaic properties of MWO_4 (M= Zn, Mg, Ca, Sr) compounds, *J. Solid State Chem.*, 2011, 184, 2103-2107, DOI: 10.1016/j.jssc.2011.06.005

21. U.S. Veerasamy, S. Palani, Y. Fujita, Y. Matsunaga, T. Kuzuya, C. Sekine and Y. Mona, Synergistic effect of MWCNT enriched $MgWO_4$ hybrid electrode for practical device assisted pouch type asymmetric supercapacitor devices, *Adv. Sens. Energy Mater.*, 2025, 100169, DOI: 10.1016/j.asems.2025.100169

22. M. Guo, G. Dou, Y. Li and S. Gong, The improvement research on microwave dielectric properties of magnesium tungstate for LTCC, *J. Mater. Sci.: Mater. Electron.*, 2015, 26, 608-612, DOI: 10.1007/s10854-014-2442-9

23. J. Thangala, S. Vaddiraju, S. Malhotra, V. Chakrapani and M. K. Sunkara, A hot-wire chemical vapor deposition (HWCVD) method for metal oxide and their alloy nanowire arrays, *Thin Solid Films*, 2009, 517, 3600-3605, DOI: 10.1016/j.tsf.2009.01.051

24. E. N. Sota, F. C. Ros and J. Hassan, Synthesis and characterisation of AWO_4 (A= Mg, Zn) tungstate ceramics, In *J. Phys. Conf. Ser., IOP Publishing,* 2018, 1083, 012002, DOI: 10.1088/1742-6596/1083/1/012002

25. N. Hurley, S. Srinivas, J. Fang, M. Sun, S. Hong, C. T. Chien, A. Guo, T. A. Khan, M. Li, M. Cotlet and F. Moretti, Investigation of the photoluminescent properties, scintillation behaviour and toxicological profile of various magnesium tungstate nanoscale motifs, *R. Soc. Open Sci.*, 2022, 9, 220994, DOI: 10.1098/rsos.220994

26. V. D. Mote, Y. P. Purushotham and B. N. Dole, Williamson-Hall analysis in estimation of lattice strain in nanometer-sized ZnO particles, *J. Theor. Appl. Phys.,* 2012, *6*, 6, DOI: 10.1186/2251-7235-6-6

27. K. A. Aly, N. M. Khalil, Y. Algamal and Q. M. Saleem, Lattice strain estimation for $CoAl_2O_4$ nano particles using Williamson-Hall analysis, *J. Alloys Compd.*, 2016, 676, 606-612, DOI: 10.1016/j.jallcom.2016.03.213

28. A. K. Zak, W. A. Majid, M. E. Abrishami and R. Yousefi, X-ray analysis of ZnO nanoparticles by Williamson–Hall and size–strain plot methods, *Solid State Sci.*, 2011, 13, 251-256, DOI: 10.1016/j.solidstatesciences.2010.11.024

29. N. Madhu, D. N. Rajendran and J. K. Thomas, A Study on the compatibility of AWO_4 nanoceramics (A= Zn, Mg and Mn) for applications in energy storage devices, In *J. Phys. Conf. Ser., IOP Publishing,* 2025, 2995, 012011, DOI: 10.1088/1742-6596/2995/1/012011

30. A. P. Amrute, J. De Bellis, M. Felderhoff and F. Schüth, Mechanochemical synthesis of catalytic materials, *Chem. Eur. J.*, 2021, 27, 6819-6847, DOI: 10.1002/chem.202004583

31. S. Dey, R. A. Ricciardo, H. L. Cuthbert and P. M. Woodward, Metal-to-metal charge transfer in AWO_4 (A= Mg, Mn, Co, Ni, Cu, or Zn) compounds with the wolframite structure, *Inorg. Chem.*, 2014, *53*, 4394-4399, DOI: 10.1021/ic4031798

32. N. Krutyak, V. V. Mikhailin, D. Spassky, I. A. Tupitsyna and A. M. Dubovik, Luminescent properties of $MgWO_4$ crystals, *IEEE International Conference on Oxide Materials for Electronic Engineering (OMEE)* 2012, 235-236, DOI: 10.1109/OMEE.2012.6464745

33. M. Zhang, J. A. Veerabhadrappa, S. F. Shaikh and A. Kumar, The Intrinsic Relationship between Photoluminescence and Photocatalysis of $MMoO_4/MWO_4$ (M= Mg, Ca, Sr and Ba) Heterojunctions: Heterojunction Construction, Mechanism Insight and Development Tendency, *Micromachines*, 2024, 15, 878, DOI: 10.3390/mi15070878

34. L. S. Kumari, P. P. Rao, A. N. P. Radhakrishnan, V. James, S. Sameera and P. Koshy, Brilliant yellow color and enhanced NIR reflectance of monoclinic $BiVO_4$ through distortion in VO_4^{3-}

tetrahedra. *Sol. Energy Mater. Sol. Cells.*, 2013, 112, 134-143, DOI: 10.1016/j.solmat.2013.01.022

35. S. Sameera, P. P. Rao, V. James, S. Divya and A. K. Raj, Influence of $(LiLa)_{1/2}MoO_4$ substitution on the pigmentary properties of $BiVO_4$, *Dyes Pigm.*, 2014, *104*, 41-47, DOI: 10.1016/j.dyepig.2013.12.029

36. S. Sameera, P. P. Rao, S. Divya, A. K. Raj and T. A. Thara, High IR reflecting $BiVO_4$-$CaMoO_4$ based yellow pigments for cool roof applications, *Energy Build.*, 2017, 154, 491-498, DOI: 10.1016/j.enbuild.2017.08.089

37. S. D. Dolić, D. J. Jovanović, D. Štrbac, L. Đ. Far and M. D. Dramićanin, Improved coloristic properties and high NIR reflectance of environment-friendly yellow pigments based on bismuth vanadate, *Ceram. Int.*, 2018, 44, 22731-22737, DOI: 10.1016/j.ceramint.2018.09.057

38. S. A. R. A. Cerro, M. Llusar, C. Gargori and G. Monrós, Cool and photocatalytic yellow ceramic pigments; from lead-tin to Cr doped scheelite pigments, *Ceram. Int.,* 2019, 45, 4613-4625, DOI: 10.1016/j.ceramint.2018.11.150

39. T. A. Thara, P. P. Rao, A. K. Raj and T. S. Sreena, New series of brilliant yellow colorants in rare earth doped scheelite type oxides, $(LiRE)_{1/2}WO_4$-$BiVO_4$ for cool roof applications, *Sol. Energy Mater. Sol. Cells*, 2019, 200, 110015, DOI: 10.1016/j.solmat.2019.110015

40. P. K. Thejus and K. G. Nishanth, Rational approach to synthesis low-cost $BiVO_4$–ZnO complex inorganic pigment for energy efficient buildings, *Sol. Energy Mater. Sol. Cells,* 2019, *200*, 109999, DOI: 10.1016/j.solmat.2019.109999

41. V. Elakkiya and S. Sumathi, Low-temperature synthesis of environment-friendly cool yellow pigment: Ce substituted $SrMoO_4$, *Materials Letters*, 2020, *263*, 127246, DOI: 10.1016/j.matlet.2019.127246

42. S. M. Thomas, S. Balamurugan, S. A. Ashika and T. S. Fathima, Micro-structural, thermal and optical properties of nanostructured CaMoO4 materials screened under different processes, *Results Chem.*, 2023, *5*, 100823, DOI: 10.1016/j.rechem.2023.100823

43. S. Balamurugan, S. M. Thomas, S. A. Ashika and T. S. Fathima, Profound impact on different properties of calcium tungstate scheelite, $CaWO_4$ phase stabilized via wider synthesis conditions, *Inorg. Chem. Commun.*, 2023. *155*, 111090, DOI: 10.1016/j.inoche.2023.111090

44. S. Balamurugan, K. S. Mini, T. S. Raja and P. Parthiban, Mechano-thermal synthesis and characterization of $BaMnO_3$ nano-needles, *J. Nanosci. Nanotechnol.*, 2015, *15*, 5978-5986, DOI: 10.1166/jnn.2015.10196

45. S. Balamurugan, B. C. Brightlin, and V. Sherly Arputha Kiruba, Synthesis of $BaFe_{12}O_{19}$ materials by mechano-thermal route: novel inorganic pigment with high near-infrared reflectance, *J. Nanosci. Nanotechnol.*, 2015, *15*, 9494-9499, DOI: 10.1166/jnn.2015.10335

46. K. M. Shri, S. Balamurugan, S. A. Ashika, T. K. Sana Fathima and N. Palanisami, Oxalic acid-derived combustion synthesis of multifunctional nanostructured copper oxide materials. *Emergent Mater.*, 2021, 4, 1387-1398, DOI: 10.1007/s42247-021-00269-4

View Article Online
DOI: 10.1039/D6MR00044D

Table 1. Micro-structural features of different $MgWO_4$ phase materials obtained through various methods from the cited work.

Synthesis method	Morphology	Particle size/shape	Ref.
Electrospinning	Fibers	-	[2]
Co-precipitation	Rod like morphology	-	[3]
Solid state reaction	Uneven grains (agglomerated)		[12]
Polymerization	Non-uniform agglomerated particles	-	[16]
Gamma-ray irradiation assisted polyacrylamide gel method	Irregular shape	150 and 220 nm	[19]
Hydrothermal	Flake shaped morphology	-	[21]
Hydrothermal	Spherical nanoparticles (small/large), wool balls, and stars	-	[25]

Table 2. NIR spectral features of different scheelites and its derived composition obtained through various methods from the cited work.

Scheelites and their derived compositions	Experimental Method	Conditions employed	NIR spectral features	Ref.
$BiVO_4$	Conventional ceramic	Calcined at 800 °C/ 9 h	46%	[34]
$BiVO_4$	Conventional solid state reaction route	Dried at 100 °C/ 1 h; calcined at 800°C/ 6 h	□50%	[35]
$(BiV)_{0.2}(CaMo)_{0.8}O_4$	Conventional solid-state route	Calcined at 800 °C/6 h	91%	[36]
$BiVO_4$	Ethylene glycol-assisted	dried in oven at 110°C for 24 h	≥80%	[37]
$BiVO_4$	Citrate-gel	heated at 150°C for 1 h; calcined at 500°C for 3 h	75.94%	[40]

$SrMoO_4$	Low temperature hydrothermal	150°C for 16 h	70%	[41]
$CaMoO_4$	Ball-milling	300 rpm/10 h	37%	[42]
	Co-precipitation	Dried at 100°C / 5 h	□85%	
$CaWO_4$	Solid state reaction	850°C/4 h	90%	[43]
	Ball-milling	300 rpm / 10 h under different conditions≠	40 - 50%	

Note: ≠ = Different amount (1.5, 3, 6, and 9.0 g) of reaction mixtures ball-milled (300 rpm / 10 h) using 3 and 30 balls of WC with 20- and 10-mm diameters, respectively.

View Article Online
DOI: 10.1039/D6MR00044D

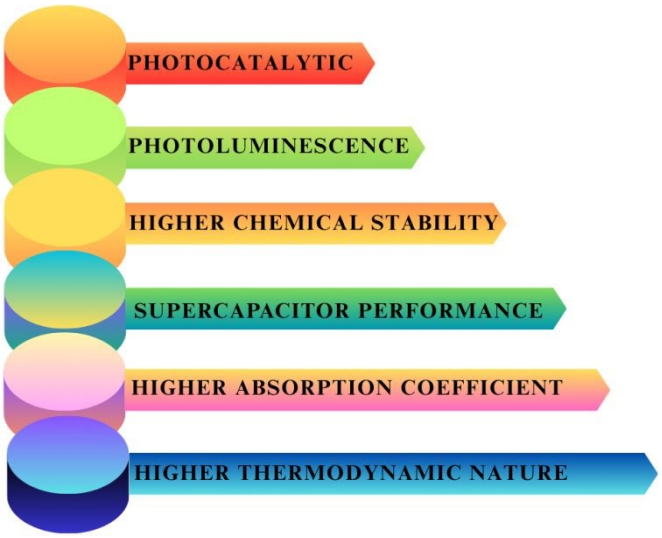

Figure 1. Characteristics of monoclinic $MgWO_4$ phase materials screened from the cited work.

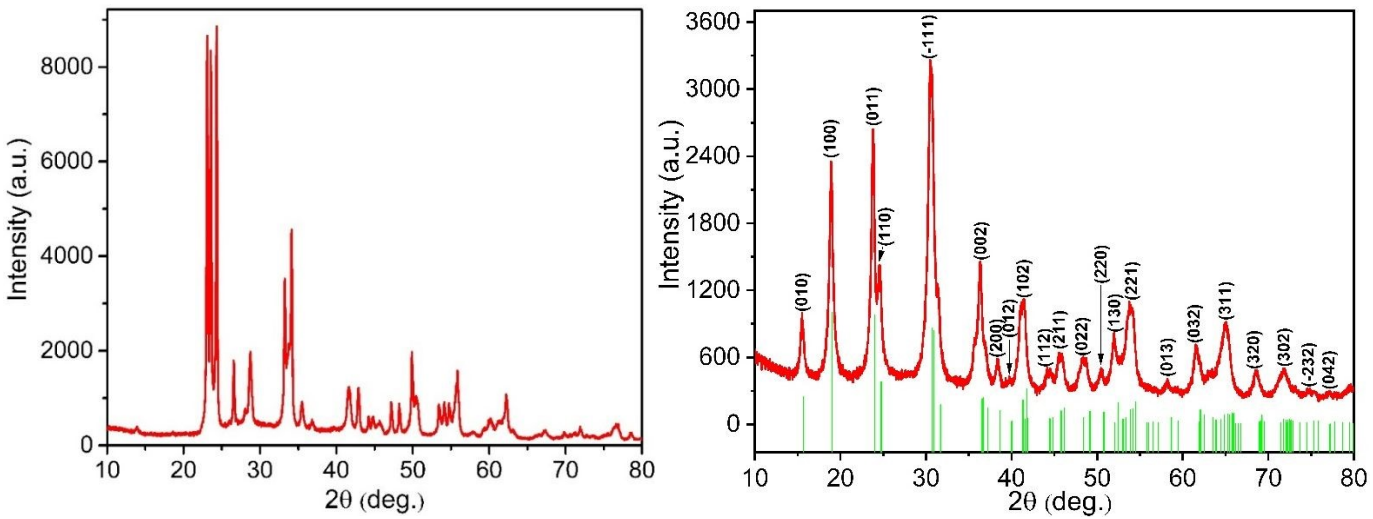

Figure 2. XRD patterns: Reaction mixture of $MgWO_4$ powder (left) and as-milled monoclinic $MgWO_4$ phase powder (right). The diffraction peaks observed in the ball-milled sample are matched with the standard data (PDF card No. 01-080-0129).

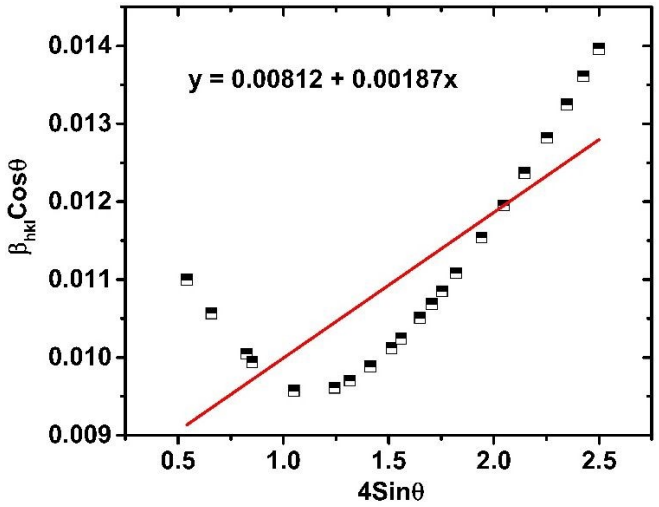

Figure 3. W-H plot for the as-milled monoclinic $MgWO_4$ phase powder.

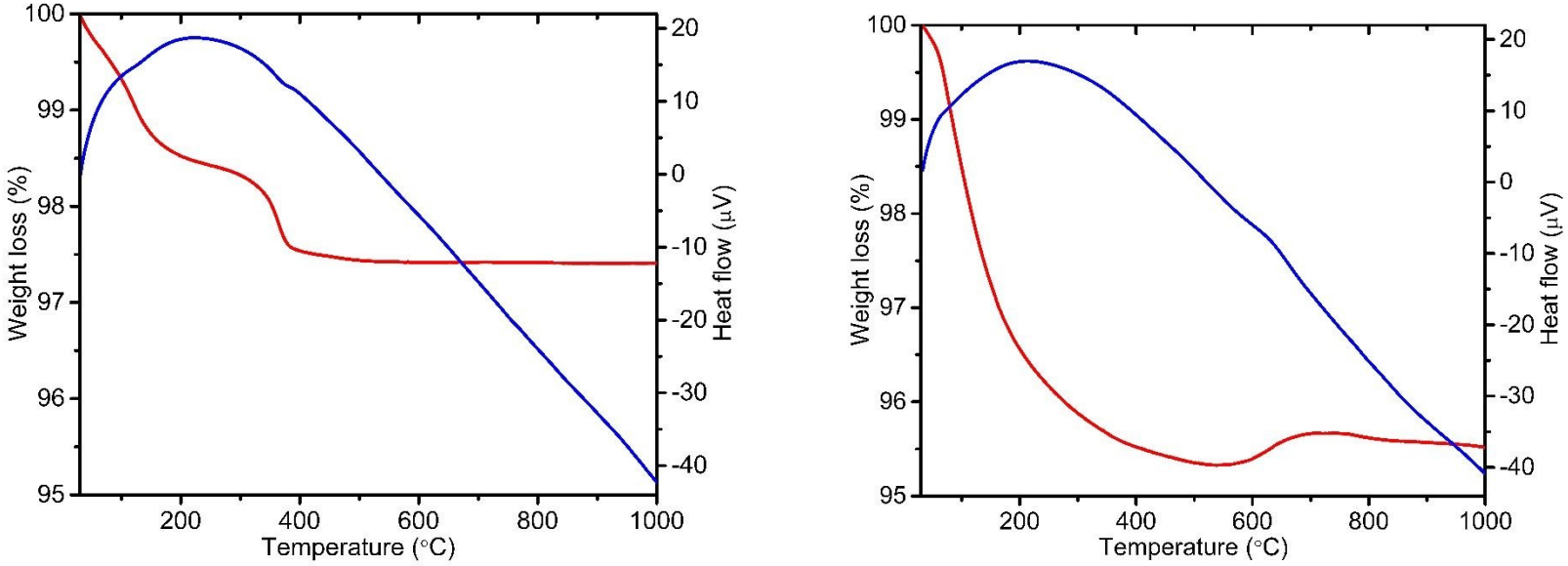

Figure 4. TGA and DTA plots: Reaction mixture of $MgWO_4$ powder (left) and as-milled monoclinic $MgWO_4$ phase powder (right).

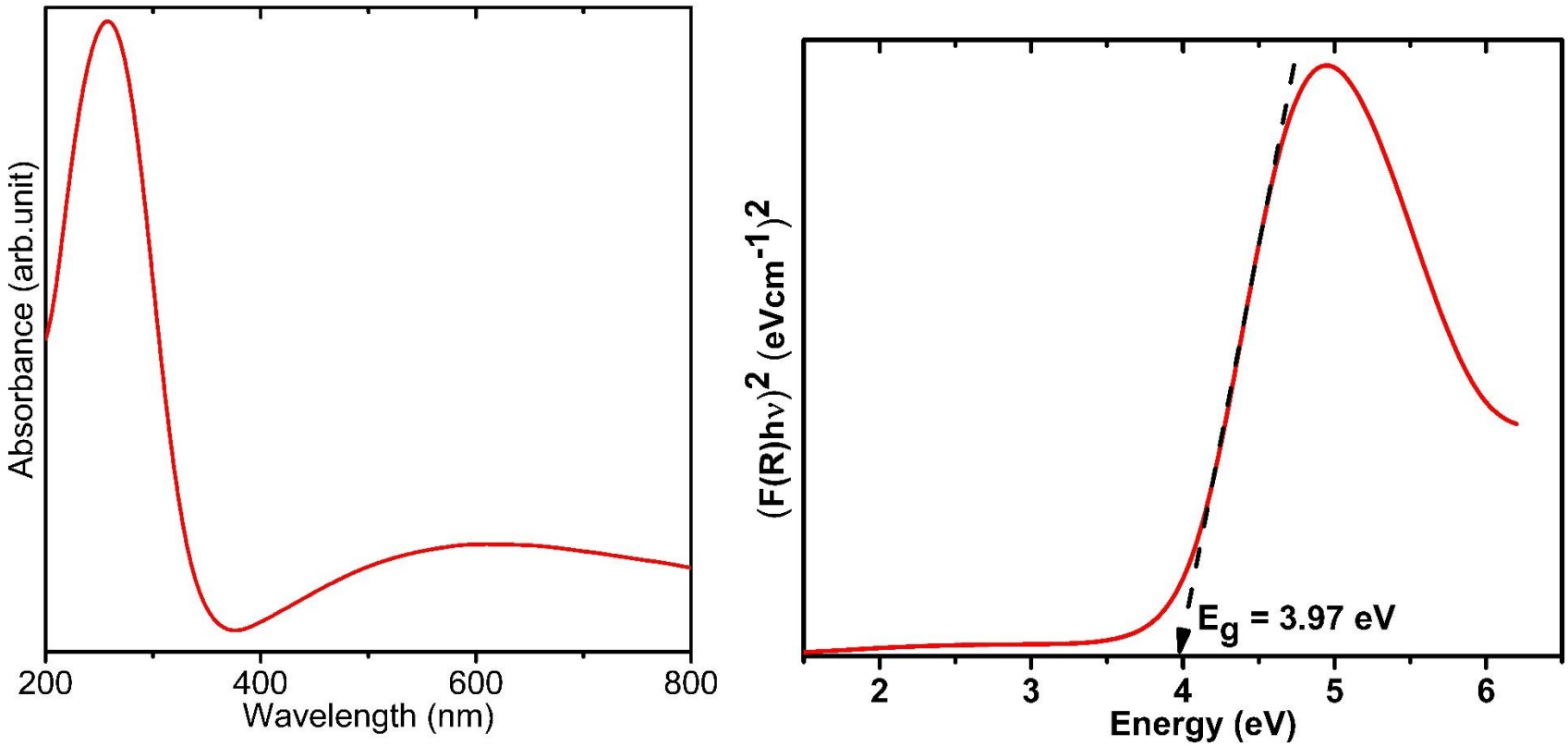

Figure 5. UV-Vis absorbance spectrum (left) and E_g^{direct} estimation from KM function (right) of the as-milled monoclinic $MgWO_4$ powder.

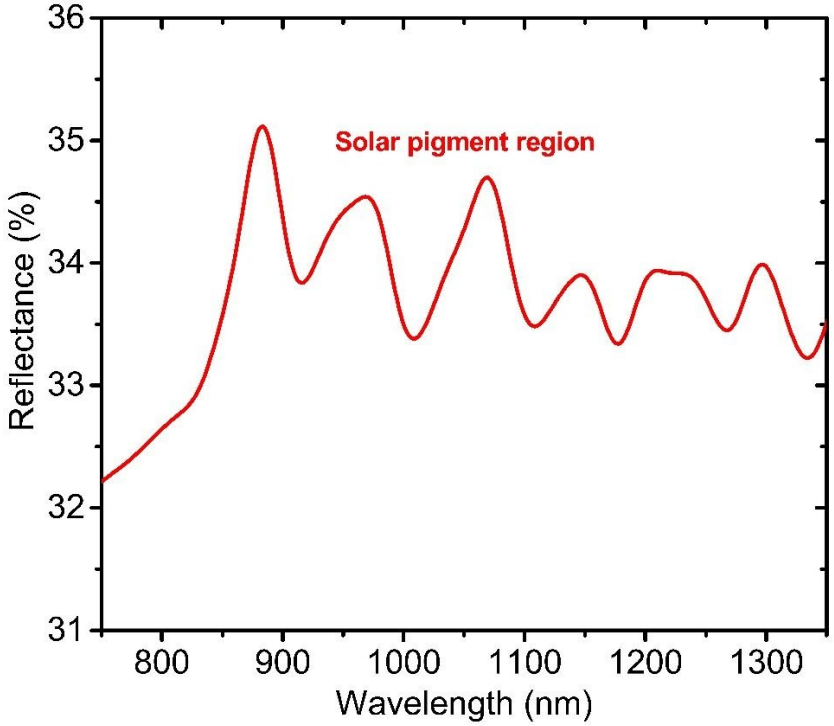

Figure 6. NIR (reflectance) spectrum of as-milled monoclinic $MgWO_4$ phase powder in the solar NIR region.

.

View Article Online
DOI: 10.1039/D6MR00044D

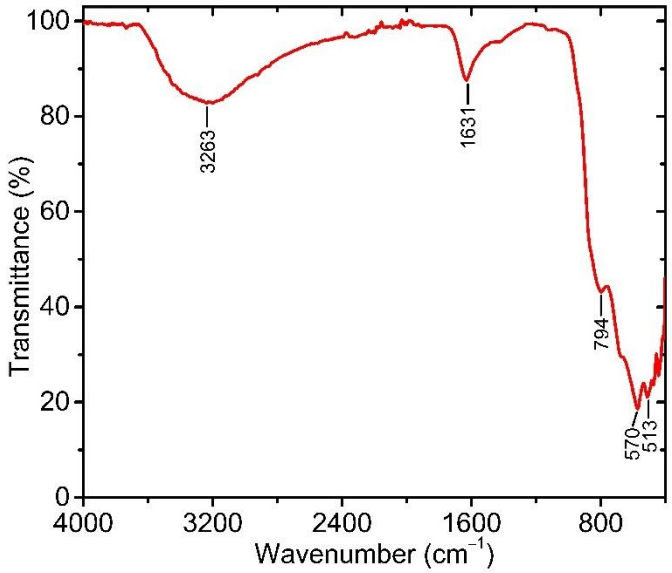

Figure 7. FTIR spectrum of as-milled monoclinic $MgWO_4$ phase powder.

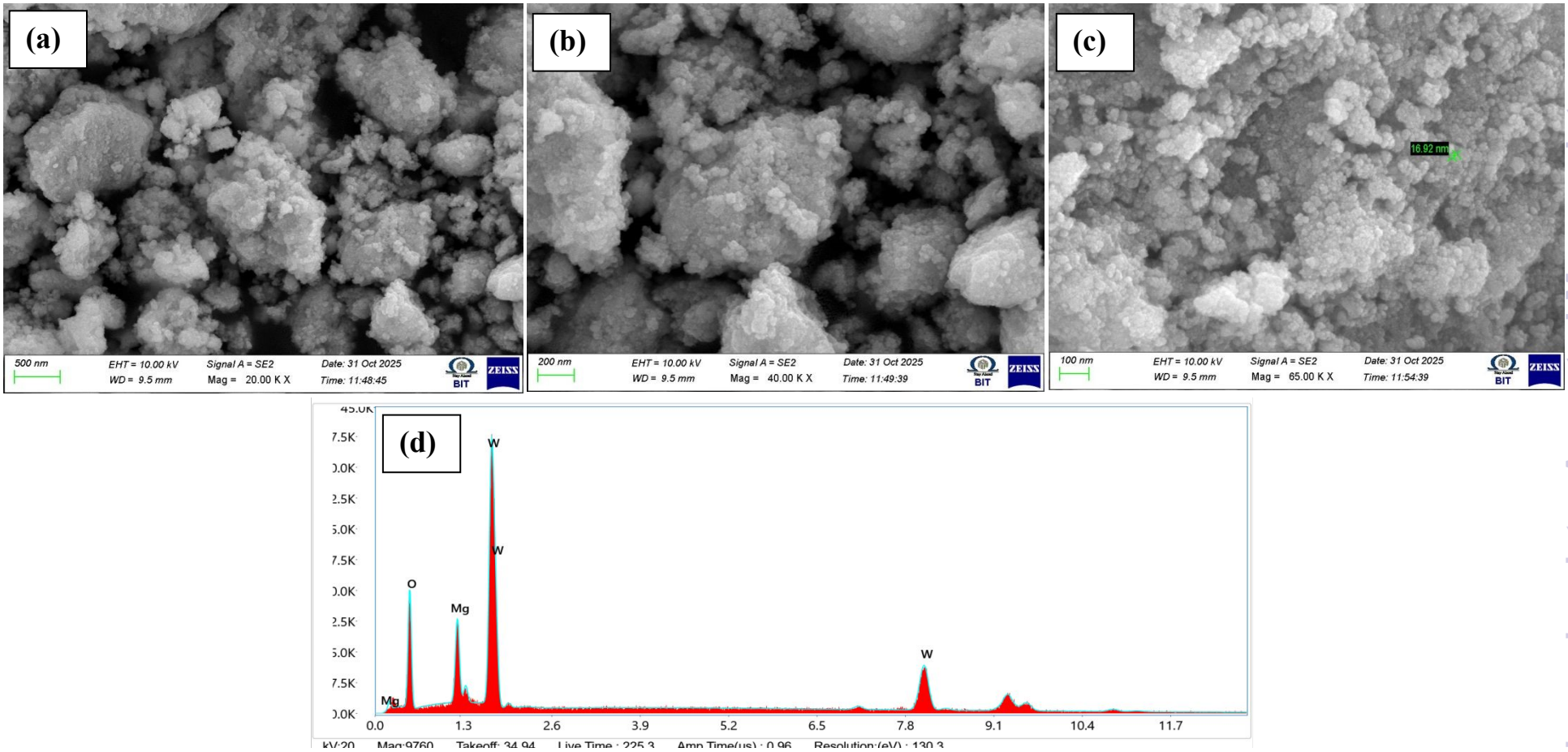

Figure 8. FESEM micro-images of the as-milled monoclinic $MgWO_4$ powder: Images were taken under the magnifications of 20000 x (a), 40000 x (b), 65000 x (c), and EDX spectrum (d).

Data Availability Statement

View Article Online
DOI: 10.1039/D6MR00044D

All relevant data generated and analyzed during this study are included in this article.